SONO-ELECTROCHEMICAL PULSE DEPOSITION OF NiP COMPOSITE COATINGS

Katya Ignatova, Daniela Lilova

University of Chemical Technology and Metallurgy
Faculty of Chemical Technologies
Department of Inorganic and Electrochemical Productions
8 Kliment Ohridski Blvd., Sofia 1797, Bulgaria, katya59ignatova@gmail.com (K.I.); lilova@uctm.edu (D.L.).

Received 09 May 2025
Accepted 29 April 2026 *DOI: 10.59957/jctm.v61.i4.2026.9*

ABSTRACT

The growth rate, elemental composition and morphology of electrodeposited NiP composite coatings in pulse mode with ultrasound stirring were investigated. NiP(C) composite coatings include graphite (C) and NiP(Prts) coatings - oxide bimetallic particles Prts, mainly of SnO and NiO. When increasing the temperature to 60 - 70°C at a concentration of graphite in the solution of 2 g L^{-1}, the growth rate of the coatings decreases compared to that at room temperature (from 11 - 13 to 8 9 mg cm^{-2} h^{-1}). The application of ultrasonic stirring and higher temperatures (60 - 70°C) increases the phosphorus content in the NiP(C) coatings to 16.38 wt. % P. In the same conditions, a coarsening of the structure of NiP(C) coatings is observed. NiP(Prts) coatings grow slower than those with graphite particles and are composed of nanosized spheroidal crystals. At higher content of bimetallic oxide particles in the solution, deposited NiP(Prts) coatings double their tin content at the expense of nickel (33.12 wt. % Ni, 15.95 wt. % P, 42.34 wt. % Sn), making the coating suitable for application as an anode material in Li-ion batteries.

Keywords: NiP, composite coatings, ultrasonic stirring, electrochemical deposition, pulse mode.

INTRODUCTION

In the last two decades, interest in transition metal phosphides prepared by electrochemical or pyrometallurgical methods has increased [1 - 3]. It has been proven that the implantation of phosphorus in the metal matrix of Ni and Co alloys leads to an increase in wear-resistance, frictional abilities and corrosion resistance of the coatings, which is why they are used in machine building, automotive, chemical and petroleum industries [1 - 4].

Transition metal phosphides have a wide range of properties that strongly depend on the composition of the phosphide and can be semiconductors, ferromagnets, catalytic materials, battery materials, etc. [5 - 8]. Thus, Ni_2P is one of the most active catalytic materials for hydrodesulfurization (HDS) and for hydrodenitrogenization (HDN) [9, 10], while NiP_2 is a promising material for the negative electrode in Li-ion batteries [11, 12]. Fe_3P is a ferromagnetic material with a high-temperature transition [13], while Fe_2P has semiconductor properties [14]. Transition metal phosphides are good catalytic materials with excellent efficiency in the hydrogen and oxygen evolution reactions during the water decomposition process [15 - 19].

In recent years, materials based on transition metals have been studied and applied in electrochemical energy storage devices such as supercapacitors, solar cells, lithium-ions, LIBs and sodium-ions batteries, NaIBs [20 - 23]. These materials are characterized by lower prices and high volumetric and gravimetric capacity [20]. Their advantage over graphite anodes, besides the high capacity, is also the lower volume expansion, which strongly affects the battery life. Among metal phosphides, nickel phosphides such as Ni_3P, Ni_2P, $Ni_{12}P_5$, Ni_5P_4, NiP_2 and NiP_3 are the most studied materials as LIBs anodes due to the richness of their phase diagram. The P - rich phases (NiP_2 and

NiP_3) have higher capacity [22]. Li implantation and reverse release from Co3P, used as an anode in LIBs show specific capacity of 400 mAh g^{-1} [24]. A NiCoP ternary alloy consisting of phosphides of both metals and with good electrochemical characteristics for Li-ions batteries was electrochemically obtained [25]. The implantation of graphite particles in NiP coatings would improve anode performance in Li-ion batteries or reveal new applications [21].

The electrochemical mechanism of NiP coating deposition has been studied in solutions containing phosphoric oxoacids as a phosphorous carrier [27 - 29]. Two possible deposition mechanisms have been proposed:

- direct through the reduction of nickel, hydrogen and hypophosphite ions [27, 28] and

- indirect - through the involvement of intermediate product phosphine in the production and implantation of phosphorous [27].

With a higher content of sodium hypophosphite, it is possible to obtain NiP by including a chemical mechanism such as reduction of Ni ions from hypophosphite anions and obtaining P by decomposition of hypophosphite [30].

The use of pulse electrolysis simultaneously with ultrasonic stirring of a suspension of graphite particles has not been well studied, although it would have a beneficial effect on the properties of the deposited composite coatings. Data about sono-electrochemical pulse deposition of Ni(SiC) composite are published in [31].

The presented paper aimed to develop an electrolyte for electrodeposition of composite NiP coatings with incorporated graphite and bimetallic oxide particles using pulse mode, with and without ultrasound stirring of the electrolyte and to determine the effect of applied conditions on the growth rate of the coatings, their elemental composition and morphology.

EXPERIMENTAL

Sono-electrochemical deposition

Composite NiP(C) and NiP(Prts) coatings were deposited on copper foil with a surface area of 4 cm^2 (2 × 2 cm) in different electrolyte compositions and by applying ultrasonic stirring and pulse potentiostatic mode. A thermostatic Digital Ultrasonic Cleaner CD-4830 with capacitance of 3000 ml and a frequency of 36 kHz was used. The bubbles, formed inside the solution at high frequency are the cause for the stirring effect realized with the device.

The deposition was performed in pulse potentiostatic mode at a frequency of 500 Hz (pulse filling $\theta = 0.5$) and an average polarization of 1.96 - 2.06V. The temperature of the electrolyte was maintained with an ultrasonic thermostatic bath in the range of 20°C - 70°C. The electrolyte with added graphite powder or powder mixture $NiO_{0.45}NiS_{0.25}SnS_{0.30}$ with a concentration of 2 - 3 g L^{-1} is subjected to heating to a suitable temperature and ultrasonic stirring for 20 - 30 min. before the start of the electrolysis. The sonication was continued during the electrolysis in the ultrasonic stirring experiments.

Pretreatment of the electrodes [32]

Copper foil was used to prepare working electrodes. They were in the shape of a rectangle measuring 1 by 2 cm. The non-working side was isolated with nitrocellulose lacquer. Before each experiment, the electrodes were subjected to pretreatment operations to clean possible contaminants and oxides on their surface: degreasing in an alcohol-ether mixture, washing in hot distilled water (80°C), glossy etching in a mixture of concentrated acids (HNO_3 : H_2SO_4 = 2 : 1) with an addition of 10 mL c. HCl in 100 ml of solution and subsequent rinsing with distilled water repeatedly. The platinum counter electrode was periodically left submerged for 5 - 10 min in a solution of 50 % HNO_3 heated to 50°C. After deposition, the coated electrodes were rinsed with distilled water and dried.

Morphological and elemental analysis

As in our previous study, the surface morphology of the samples was analysed by Scanning Electron Microscopy (SEM) using an SEM/FIB LYRA I XMU microscope of the company TESCAN with tungsten heated filament as an electronic source, 3.5 nm resolution at 30 kV and accelerating voltage from 200 V up to 30 kV [32]. The microscope was equipped with an EDX detector Quantax 200 of the company BRUKER for quantitative analysis. Spectroscopic resolution at Mn-Kα and 1 kcps 126 eV was used.

Electrolyte preparation

The electrolyte we developed and applied had the following composition: 0.3M $NiSO_4$, 0.6M H_3PO_3, 0.06M NaH_2PO_2, 30 g L^{-1} Na_2SO_4. The pH of solution

was 3.5 and the temperature was 20 - 70°C, maintained with the thermostatic device of the ultrasound bath. The deposition of NiP(C) and NiP(Prts) is carried out in the same electrolyte composition with the addition of the corresponding powder materials. Fine graphite powder for NiP(C) coatings is based on soft carbon (type Soft) and is characterized by parallel arranged graphene layers with a high degree of defects, an average particle size of 3 - 8 μm, and is suitable for use in lithium-ion batteries [33]. For NiP(Prts) coatings, a bimetal powder, (designated as Prts) was used.

Growth rate of the coating mass

The growth rate (GR) of the coating mass is estimated by the Eq. (1):

$$GR = m_2 - m_1 = \Delta m/S.t_{el}\ ,\ mg/cm^2\,h \qquad (1)$$

where m_1 [mg] is the mass of the electrode before electrolysis, m_2 [mg] - the mass of the electrode after electrolysis, S - electrode surface, cm^2 and t_{el}, h is the time for which the electrolysis itself is carried out.

RESULTS AND DISCUSSION

Synthesis and characterization of bimetallic powder (Prts) for deposition of NiP(Prts) coatings

The bimetallic powder (Prts) was prepared by controlled heating of a solution of $NiSO_4$, $SnCl_2$ and 50 g L^{-1} sodium gluconate ($C_6H_{11}NaO_7$) to 80 - 90°C (pH = 2-3). The resulting powder mixture was washed, dried and ground in an agate mortar for homogenization and then quantities of it were introduced into the electrolyte to obtain composite NiP(Prts) coatings.

According to the X-ray analysis (Fig. 1), the latter consists of 44.90 wt. % NiO(OH); 14.45 wt. % SnS; 17.96 wt. % SnO and 22.45 wt. % S (Fig.1). The material was obtained by controlled heating of a solution of $NiSO_4$, $SnCl_2$ and 50 g L^{-1} sodium gluconate ($C_6H_{11}NaO_7$) up to 80 - 90°C (pH = 2 - 3). The resulting powder mixture was rinsed, dried and ground in an agate mortar to homogenize, and then a certain amount was introduced into the electrolyte to obtain NiP(Prts) composite coatings. The results for the composition of the material "Prts" from X-Ray data are in excellent agreement with those from EDX and EDX-Mapping analyses shown in Fig. 2.

SEM image in Fig. 2a shows that the "Prts" material is very finely crystalline and is characterized by an average crystallite size of about 1 μm.

Data on the rate of growth of coatings GR_m, mg $cm^{-2}\,h^{-1}$ and elemental composition in wt. % by respective experimental conditions: temperature of electrolyte, t°C, ultrasonic stirring, US and concentration of graphite, C or bimetallic particles, Prts in electrolyte, g L^{-1} are presented in Table 1.

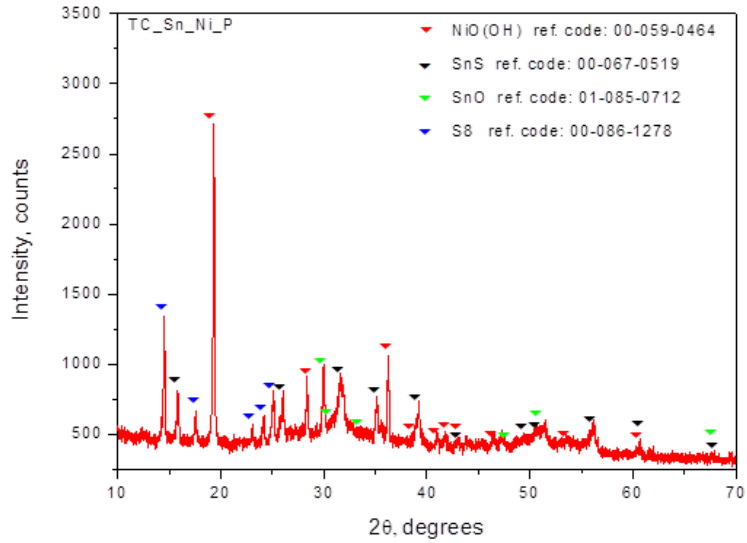

Fig.1. X-Ray diffractogram of the material, described as „Prts"($NiO_{0.45}$ $NiS_{0.25}SnO_{0.30}$), used for electrodeposition of NiP(Prts) composite coatings.

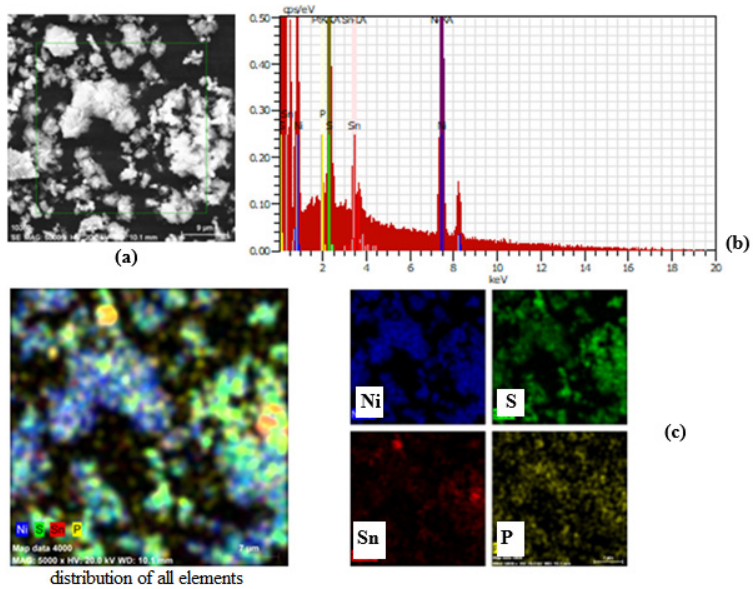

Fig. 2. SEM image (a), EDX spectrum (b) and SEM-mapping (c) of the „Prts" - material.

Table 1. Elemental composition in wt. %, growth rate of coatings GR_m, mg cm^{-2} h^{-1} at respective experimental conditions: temperature of the electrolyte, t°C, ultrasonic stirring, US and concentration of graphite, C or bimetallic particles, Prts in electrolyte, g L^{-1}.

Nr	alloy	t, °C	Ultrasonic stirring, "+" US; Content of Gr or Prts in g L^{-1}	GR_m, mg cm^{-2} h^{-1}	Ni, wt. %	P, wt. %	Sn, wt. %	C, wt. %	O, wt. %
1	NiP(C)	20	- US (2 g L^{-1} Gr)	11.86	82.38	13.12	-	2.06	2.44
2	NiP(C)	20	+ US (2 g L^{-1}Gr)	12.64	87.5	2.00	-	5.34	5.16
3	NiP(C)	60	+ US (2 g L^{-1} Gr)	8.320	80.02	8.19	-	6.83	4.25
4	NiP(C)	70	+ US (2 g L^{-1} Gr)	9.024	79.18	16.38	-	2.13	2.33
5	NiP(Prts)	60	+ US (2g L^{-1}Prts)	4.8	70.35	7.99	19.09	-	3.21
6	NiP(Prts)	60	+ US (3g L^{-1}Prts)	2.016	33.12	15.95	42.34	-	8.59

NiP(C)

Table 1 shows that at graphite content of 2 g L^{-1} in the solution, the growth rate of the coating mass, GR is higher at a lower temperature of 20°C (11.86 mg cm^{-2} h^{-1} at "quiet" conditions and 12.64 mg cm^{-2} h^{-1} at ultrasound stirring). Increasing the temperature to 60 - 70°C at the same graphite content in the solution leads to a lower r_m of 8 - 9 mg cm^{-2} h^{-1}.

As can be seen from Table 1, under "quiet" conditions, 20°C and content of graphite particles of 2 g L^{-1} (sample 1), a high content of Ni (82.38 wt. %), as well as P (13.12 wt. %) were found. The application of ultrasound under the same other conditions (sample 2) leads to a decrease in phosphorus content to 2.00 wt. %. When using higher temperatures (60 - 70°C) and a concentration of graphite in the solution of 2 g L^{-1}, the phosphorus content in the coating increases to 16.38 wt. % P (sample 4).

As can be seen from Fig. 3 under the investigated conditions an important change in the morphology of the deposited coatings was found. The coating obtained under "quiet" conditions (sample 1 from Table 1) has a fine crystalline structure but with very uneven deposition of graphite particles (Fig. 3a, a*). Dark non-uniform

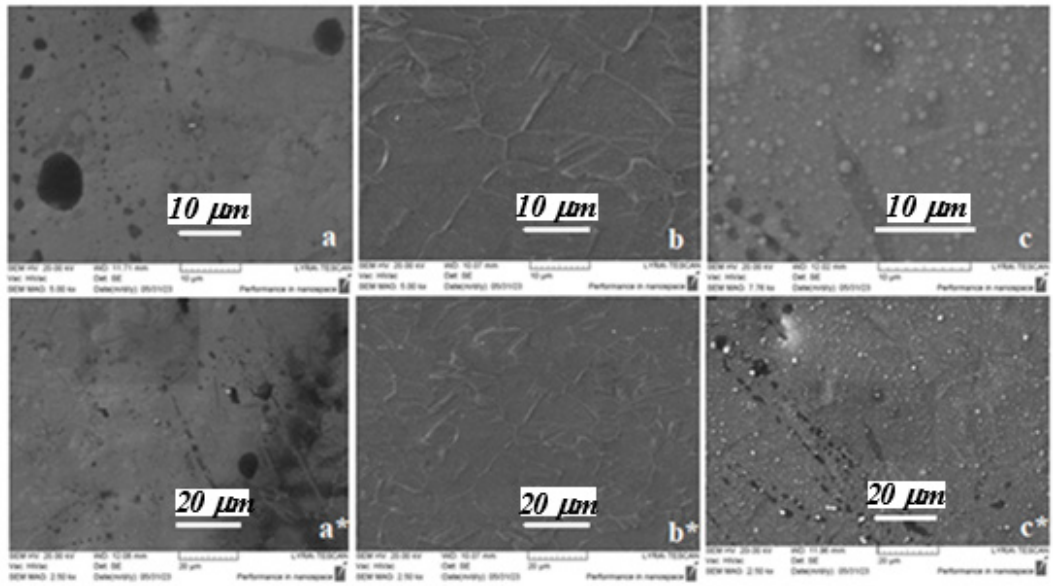

Fig. 3. SEM images of NiP(C) coatings at two different magnifications: (a, a*) - sample 1 from Table 1; (b, b*) - sample 2 from Table 1; (c, c*) - sample 4 from Table 1.

spots are visible on the surface. As can be seen from Fig. 3b, b* (sample 2 from Table 1) the application of ultrasound stirring at low temperature (20°C) leads to the formation of dark lines on the coatings. When the temperature rises to 60°C, the coating's structure becomes rougher with the formation of spheroidal crystals (Fig. 3c, c*).

NiP (Prts)

Table 1 shows that the growth rate of the NiP(Prts) coating is 4.8 mg $cm^{-2} h^{-1}$ in a solution with a concentration of Prts of 2 g L^{-1} and 2.016 mg $cm^{-2} h^{-1}$ when the same is 3 g L^{-1}. The rate of growth of coatings is influenced by a complex of factors, among which are the electrical conductivity of the solution, the electrophoretic speed of the particles depending on their size and charge, and polarization effects at the electrode-solution interface. The listed factors change as the concentration of bimetallic oxide particles in the electrolyte varies, especially with ultrasonic stirring. In such systems, defined as suspensions, the thickness of the diffusion layer is expected to decrease upon sonication of the electrolyte, which should increase the mass growth rate of the coatings. Our results confirm adherence to these theoretical principles [34]. The observed two-fold decrease in the growth rate of NiP(Prts) coatings with increasing bimetallic particle content in the electrolyte at constant other conditions (samples 5 and 6 in Table 1) well illustrates the above.

Fig. 4 shows SEM images of NiP alloy coatings with introduced bimetallic oxide particles. The coatings were deposited at an electrolyte temperature of 60°C and varying the content of particles in the solution. The effect of changing the particle content in the solution on the morphology of the coatings is not very noticeable. The coatings are made of nano-sized spheroidal crystallites on a smooth base.

Table 1 shows that the coating content depends strongly on the particles content. At 2 g L^{-1} Prts, coatings with a composition of 70.35 wt. % Ni, 7.95 wt. % P and 19.03 % Sn were obtained. At 3 g L^{-1} Prts, coatings with a composition of 33.12 wt. % Ni, 15.95 wt. % P and 42.34 wt. % Sn were deposited, which are very suitable for application in Li-ion batteries because the Sn/Ni ratio is above 1. Sn is known to be the active element in anodes during the electrochemical conversion of Li [35].

The images of the NiP(C) and NiP(Prts) coatings show some morphological heterogeneity, but the SEM - Mapping analyses of samples 4 (Fig. 5) and 5 (Fig. 6) show that the elements are evenly distributed on the coating's surface.

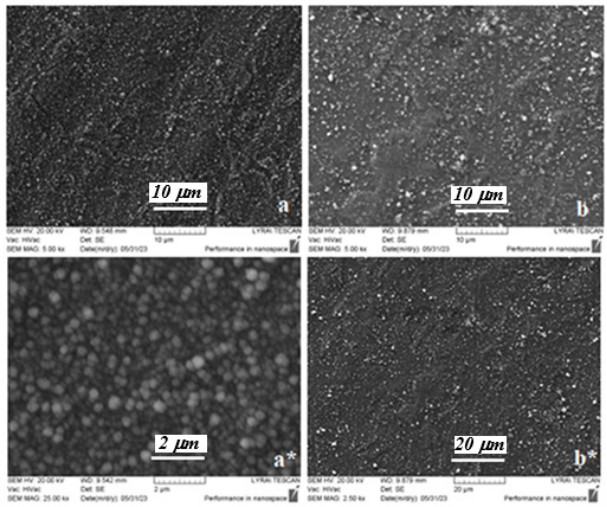

Fig. 4. SEM images of NiP(Prts) coatings at different magnifications: (a, a*) - sample 5 from Table 1; (b, b*) - sample 6 from Table 1.

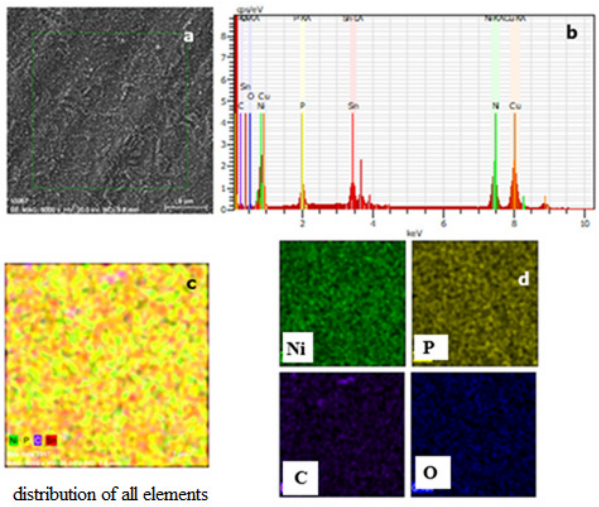

Fig. 6. SEM image (a), EDX spectrum (b), summary view of all elements (c), and discrete distribution of each of the elements (d) by SEM - Mapping analysis of NiP(Prts) coating - sample 5 from Table 1.

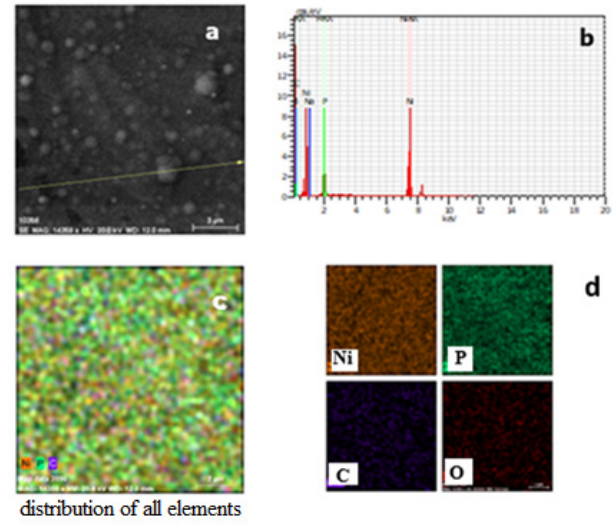

Fig. 5. SEM image (a), EDX spectrum (b), color distribution of all elements (c) and of individual elements (d) on the coating surface of NiP(C) coating - sample 4 from Table 1.

CONCLUSIONS

Based on the obtained data, the following conclusions can be drawn: For NiP(C): I) When increasing the temperature to 60 - 70°C at a concentration of graphite in the solution of 2 g L^{-1}, the growth rate of the coating decreases compared to that at room temperature; II) Application of ultrasonic stirring and higher temperatures (60 - 70°C) leads to an increase in phosphorus in the coating up to 16.38 wt. % P; III) NiP(C) coating deposited at "quiet" conditions has a fine-crystal structure but a very uneven distribution of the graphite particles. Applying ultrasonic stirring simultaneously with an increase in the temperature to 60°C gives a slightly rough structure to the coating. The elements are evenly distributed on the surface; For NiP (Prts): IV) NiP (Prts) coatings grow at a slower rate than those with graphite particles and are composed of nanosized spheroidal crystals; V) At higher content of bimetallic oxide particles in the solution, deposited NiP (Prts) coatings double their tin content at the expense of nickel (33.12 wt. % Ni, 15.95 wt. % P, 42.34 wt. % Sn), making the coating suitable for application as anode material in Li-ion batteries.

Authors' contributions

K.I.: Conceptualization, experimental work, writing - original draft and editing; D.L.: Experimental work, data collections, review.

REFERENCES

1. C. Ma, S.C. Wang, L.P. Wang, F.C. Walsh, R.J.K. Wood, The electrodeposition and characterization of low-friction and wear-resistant Co-Ni-P coatings, Surf. Coating. Technol., 235, 2013, 495-505.
2. N.M. Alanazi, A.M. El-Sherik, S.H. Alamarand, Sh.

Shen, Influence of residual stresses on corrosion and wear behavior of electrodeposited nanocrystalline Co-P coatings, Int. J. Electrochem. Sci., 8, 2013, 10350-10358.
3. C. Ma, S.C. Wang, F.C. Walsh, The electrodeposition of nanocrystalline Cobalt-Nickel-Phosphorus alloy coatings: review, Trans. IME, Int. J. Surf. Eng. Coat., 93, 5, 2015, 275-282.
4. S.J. Splinter, R. Rofangha, N.S. McIntyre, U. Erb, XPS characterization of the corrosion films formed on nanocrystalline Ni–P alloys in sulphuric acid, Surf. Interface Anal., 24, 1996, 181-186.
5. X. Wang, H. M. Kim, Y. Xiao, Y.K. Sun, Nanostructured metal phosphide-based materials for electrochemical energy storage, J. Mater. Chem. A, 4, 2016, 14915.
6. L. Sun, X. Xiang, J. Wu, Ch. Cai, D. Ao, J. Luo, Ch. Tian, X. Zu, Bi-metal phosphide NiCoP: An enhanced catalyst for the reduction of 4-nitrophenol, Nanomaterials (Basel), 9, 1, 2019, 112.
7. V. Pralong, D.C.S. Souza, K.T. Leung, L.F. Nazar, Reversible lithium uptake by CoP_3 at low potential: role of the anion, Electrochem. Commun., 4, 2002, 516-520.
8. S.L. Liu, C.L. Ma, L.B. Ma, H.Z. Zhang, Synthesis of NiCoP hollow spheres and its electrochemical property, Chem. Phys. Lett., 638, 2015, 52-55.
9. Sh. Yang, Ch. Liang, R. Prins, A novel approach to synthesizing highly active Ni_2P/SiO_2 hydrotreating catalysts, J. Catalysis, 237, 1, 2016, 118-130.
10. Y.K. Lee, Sh.J. Oyama, Sulfur resistant nature of Ni_2P catalyst in deep hydrodesulfurization, Applied Catalysis A: General, 2017, 548, 103-113.
11. Y. Lu, T. Wang, X. Li, G. Zhang, H. Xue, H. Pang, Synthetic methods and electrochemical applications for transition metal phosphide nanomaterials, RSC Advandces, 90, 2016.
12. H. Pang, Y.Z. Zhang, Z. Run, W.Y. Lai, W. Huang, Amorphous nickel pyrophosphate microstructures for high-performance flexible solid-state electrochemical energy storage devices, Nanomat. Energy, 17, 10, 2015, 339-347.
13. St. L. Brock, K. Senevirathne, Recent developments in synthetic approaches to transition metal phosphide nanoparticles for magnetic and catalytic applications, J. Sol. State Chem., 7, 2008, 1552-1559.
14. C. Mattei, PhD Dissertation, Versatile Synthesis of Transition Metal Phosphides: Emerging Front-runners for Affordable Catalysis, Virginia Commonwealth University, 2016.
15. .H. Jang, E.G. Kim, Y.H. Chung, S.J. Yoo, Y.K. Lee, The nature of active sites of Ni_2P electrocatalyst for hydrogen evolution reaction, J. Catalysis, 326, 2015, 92-99.
16. I. Paseka, Hydrogen evolution reaction on amorphous Ni-P and Ni-S electrodes and the internal stress in a layer of these electrodes, Electrochim. Acta, 47, 6, 2001, 921-931.
17. R.K. Shervedani, A. Lasia, Studies of the hydrogen evolution reaction on Ni-P electrodes. J. Electrochem. Soc., 144, 2, 1997, 511-519.
18. J.J. Podesta, R.C.V. Piatti, A.J. Arvia, The influence of iridium, ruthenium and palladium on the electrochemical behaviour of Co-P and Ni-Co-P base amorphous alloys for water electrolysis in KOH aqueous solutions, Int. J. Hydrogen Energy 20, 2, 1995, 111-122.
19. T.V. Vineesh, S. Mubarak, M.G. Hahm, V. Prabu, S. Alwarapp, T.N. Narayanan, Controllably alloyed, low density, free-standing Ni-Co and Ni-Graphene sponges for electrocatalytic water splitting, Scientific Repotrts, 2016, 31202. doi: 101038/srep312026.
20. X. Wang, H.M. Kim, Y. Xiao, Y.K. Sun, Nanostructured metal phosphide-based materials for electrochemical energy storage, J. Mater. Chem., 4, 2016, 14915-14931.
21. Y. Lu, T. Wang, X. Li, G. Zhang, H. Xue, H. Pang, Synthetic methods and electrochemical applications for transition metal phosphide nanomaterials, RSC Adv., 90, 2016.
22. H. Pang, Y.Z. Zhang, Z. Run, W.Y. Lai, W. Huang, Amorphous nickel pyrophosphate microstructures for high-performance flexible solid-state electrochemical energy storage devices, Nano Energy, 17, 10, 2015, 339-347.
23. H. Pang, Y.Z. Zhang, W.Y. Lai, Z. Hu, W. Huang, Lamellar $K_2Co_3(P_2O_7)_2 \cdot 2H_2O$ nanocrystal whiskers: high-performance flexible all-solid-state asymmetric micro-supercapacitors via inkjet printing, Nano Energy, 15, 6, 2015, 303-312.
24. V. Pralong, D.C.S. Souza, K.T. Leung, L.F. Nazar, Reversible lithium uptake by CoP_3 at low potential: role of the anion, Electrochem. Commun., 4, 2002, 516-520.

25. S.L. Liu, C.L. Ma, L.B. Ma, H.Z. Zhang, Synthesis of NiCoP hollow spheres and its electrochemical property, Chem. Phys. Lett., 638, 2015, 52-55.
26. Y. Wei, Optimization of microwave absorption properties of C/NiP microfiber composites, Ceramics Internat., 47, 6, 2021, 7937-7945.
27. A. Brenner, Electrodeposition of Alloys, vol. II, Academic Press, New York, 1963.
28. T. Morikawa, T. Nakade, M. Yokoi, Y. Fukumoto, C. Iwakura, Electrochim. Acta, 42, 1997, 115.
29. C.S. Lin, C.Y. Chen, C.T. Chien, P.L. Lin, W.C. Chung, Electrodeposition of Ni-P alloy from sulfamate baths with improved current efficiency, J. Electrochem. Soc., 153, 6, 2006, C387-C392.
30. N. Rakitevitch, PhD Thesis, Elektrochimitcheskoe dobivanie Ni-P i Ni-Co-P splavi, Universitet Pristina, 1994, (in Serbian).
31. G. Gyawali, S.H.Cho, D.J.Woo, S.W.Lee, Pulse electrodeposition and characterisation of Ni-SiC composite coatings in presence of ultrasound, Transactions, 2012, 90, 5, 274-281.
32. K. Ignatova, D. Lilova, Ultrasonic-assisted electrodeposition of SnNi(C) composite coatings, J. Chem. Technol. Metall., 60, 5, 2025, 833-841.
33. D. Saurel, J. Segalini et al., A SAXS outlook on disordered carbonaceous materials for electrochemical energy storage, Energy Storage Materials, 21, 5, 2019. https: //doi.org/10.1016/j.ensm.2019.05.007.
34. J. M. Costa, A. F. de Al. Neto, Ultrasound-assisted electrodeposition and synthesis of alloys and composite materials, Ultrasonics Sonochemistry, review, 2020, 5, 68:105193. https://doi: 10.1016/j.ultsonch.2020.105193.
35. H. Ying, W.Q. Han, Metallic Sn-Based Anode Materials, Application in High-Performance Lithium-Ion and Sodium-Ion Batteries, Adv.Sci. (Weinh), 4, 11, 2017, 1-35.